



Science Arts & Métiers (SAM)

is an open access repository that collects the work of Arts et Métiers Institute of Technology researchers and makes it freely available over the web where possible.

This is an author-deposited version published in: <https://sam.ensam.eu>
Handle ID: <http://hdl.handle.net/10985/12496>

To cite this version :

Thomas HENNERON, Stephane CLENET - Application of the Proper Generalized Decomposition to Solve MagnetoElectric Problem - IEEE Transactions on Magnetics p.1-4 - 2017

Any correspondence concerning this service should be sent to the repository

Administrator : scienceouverte@ensam.eu



with \mathbf{S} the strain tensor, \mathbf{c} the stiffness tensor, $\boldsymbol{\tau}$ the piezoelectric coefficients, ε the electric permittivity, ν the magnetic reluctivity and \mathbf{h} the relative piezomagnetic coefficients defined by $\mathbf{h}=\mathbf{e}\cdot\nu$ with \mathbf{e} the piezomagnetic coefficients. To solve the problem, a formulation in terms of potentials can be used. From (2-a) and (3-b) and by assuming small deformations, we have

$$\mathbf{E} = -\mathbf{grad}v - v_0(\mathbf{grad}\alpha_{v_1} + \mathbf{grad}\alpha_{v_2}) \quad (7)$$

$$\mathbf{B} = -\mathbf{grad}_R \mathbf{A} - \Phi \mathbf{grad}_R \alpha_A \quad (8)$$

$$\mathbf{S} = \frac{1}{2}(\mathbf{gradu} + \mathbf{grad}^t \mathbf{u}) = \boldsymbol{\mathcal{D}}\mathbf{u} \quad (9)$$

with v the electric potential defined in D , Γ_{v_1} , Γ_{v_2} , v_0 (resp. $-v_0$) the electric potential on Γ_{v_1} (resp. Γ_{v_2}), α_{v_1} and α_{v_2} scalar functions equal to 1 and -1 on Γ_{v_1} and Γ_{v_2} respectively and 0 elsewhere, \mathbf{A} the magnetic potential defined on D , Γ_{A_1} , Γ_{A_2} and α_A a scalar function equal to 1 on Γ_{A_1} , -1 on Γ_{A_2} and 0 elsewhere. Then, we seek for the solutions v , \mathbf{A} and \mathbf{u} in the space domain D and in the angular frequency interval $[\omega_{\min}; \omega_{\max}]$.

III. PROPER GENERALIZED FORMULATION

The PGD method consists in approximating the solutions by a sum of separable functions in frequency and space. Then, v , \mathbf{A} and \mathbf{u} are approximated by separated forms of space and frequency functions,

$$v \approx \sum_{j=1}^M \mathbf{R}_j^v(\mathbf{x}) S_j^v(\omega), \mathbf{A} \approx \sum_{j=1}^M \mathbf{R}_j^A(\mathbf{x}) S_j^A(\omega) \text{ and } \mathbf{u} \approx \sum_{j=1}^M \mathbf{R}_j^u(\mathbf{x}) S_j^u(\omega) \quad (10)$$

with $\mathbf{x} \in D$, $\omega \in [\omega_{\min}; \omega_{\max}]$ and M the number of modes of the expansions. To apply the PGD approach, we consider a weak formulation on $D \times [\omega_{\min}; \omega_{\max}]$ of (1), (2-b) and (3-a). In the following, we suppose that the electric charge Q is imposed. Then, we have:

$$\int_{\omega_{\min}}^{\omega_{\max}} \int_D \mathbf{u}' \cdot [\mathbf{div} \mathbf{T} + \rho \omega^2 \mathbf{u}] dD d\omega = 0 \quad (11)$$

$$\int_{\omega_{\min}}^{\omega_{\max}} \int_D v' \cdot \mathbf{div} \mathbf{D} dD d\omega = 0 \quad (12)$$

$$\int_{\omega_{\min}}^{\omega_{\max}} \int_D \mathbf{A}' \cdot \mathbf{curl} \mathbf{H} dD d\omega = 0 \quad (13)$$

$$\int_{\omega_{\min}}^{\omega_{\max}} \int_D \alpha_{v_1} \cdot \mathbf{div} \mathbf{D} dD d\omega = \int_{\omega_{\min}}^{\omega_{\max}} Q d\omega \quad (14)$$

$$\int_{\omega_{\min}}^{\omega_{\max}} \int_D \alpha_{v_2} \cdot \mathbf{div} \mathbf{D} dD d\omega = - \int_{\omega_{\min}}^{\omega_{\max}} Q d\omega \quad (15)$$

with \mathbf{u}' , v' and \mathbf{A}' test functions defined in the same spaces of the functions \mathbf{u} , v and \mathbf{A} respectively. To compute the functions \mathbf{R}_j^l and S_j^l for $j \in [1:M]$ and $l = \{v, A, u\}$ and v_0 , an iterative enrichment approach is used. At the n^{th} iteration, v_n , \mathbf{A}_n and \mathbf{u}_n are expressed as functions of \mathbf{R}_n^l and S_n^l and of the known previous approximations v_{n-1} , \mathbf{A}_{n-1} and \mathbf{u}_{n-1} such as

$$v_n = \mathbf{R}_n^v(\mathbf{x}) S_n^v(\omega) + v_{n-1}, \mathbf{A}_n = \mathbf{R}_n^A(\mathbf{x}) S_n^A(\omega) + \mathbf{A}_{n-1} \text{ and}$$

$$\mathbf{u}_n = \mathbf{R}_n^u(\mathbf{x}) S_n^u(\omega) + \mathbf{u}_{n-1}. \text{ Then, to compute the unknown}$$

functions \mathbf{R}_n^l , S_n^l and v_0 , two sets of equations deduced from (11-15) are solved iteratively. In a first step, we assume that the functions S_n^l with $l = \{v, A, u\}$ and v_0 are known in order to calculate the functions \mathbf{R}_n^l . In 2D, the functions are discretised in the nodal element space such as $\mathbf{R}_n^l = \mathbf{W}^l \mathbf{R}_n^l$ for $l = \{v, A, u\}$ with \mathbf{W} the vector which entries are the nodal functions and \mathbf{R}_n^l the vector of the values at the nodes. Then, we solve

$$\begin{bmatrix} \chi_{uu} \int_D (\boldsymbol{\mathcal{D}} \mathbf{W}^u)^t \boldsymbol{\mathcal{D}} \mathbf{W}^u - \delta_{uu} \int_D \mathbf{W}^{ut} \rho \mathbf{W}^u & \beta_{uv} \int_D (\boldsymbol{\mathcal{D}} \mathbf{W}^u)^t \boldsymbol{\tau}^t \mathbf{grad} \mathbf{W}^v & \beta_{uA} \int_D (\boldsymbol{\mathcal{D}} \mathbf{W}^u)^t \mathbf{h}^t \mathbf{grad}_R \mathbf{W}^A \\ \beta_{vu} \int_D (\mathbf{grad} \mathbf{W}^v)^t \boldsymbol{\tau} \boldsymbol{\mathcal{D}} \mathbf{W}^u & -\beta_{vv} \int_D (\mathbf{grad} \mathbf{W}^v)^t \varepsilon \mathbf{grad} \mathbf{W}^v & \mathbf{0} \\ \beta_{Au} \int_D (\mathbf{grad}_R \mathbf{W}^A)^t \mathbf{h} \boldsymbol{\mathcal{D}} \mathbf{W}^u & \mathbf{0} & \beta_{AA} \int_D v (\mathbf{grad}_R \mathbf{W}^A)^t \mathbf{grad}_R \mathbf{W}^A \end{bmatrix} \begin{bmatrix} \mathbf{R}_n^u \\ \mathbf{R}_n^v \\ \mathbf{R}_n^A \end{bmatrix} = \begin{bmatrix} - \int_{\omega_{\min}}^{\omega_{\max}} \int_D v_0 \int_D (\boldsymbol{\mathcal{D}} \mathbf{W}^u)^t \boldsymbol{\tau}^t (\mathbf{grad} \alpha_{v_1} + \mathbf{grad} \alpha_{v_2}) \\ \int_{\omega_{\min}}^{\omega_{\max}} \int_D S_n^{v*} v_0 \int_D (\mathbf{grad} \mathbf{W}^v)^t \varepsilon (\mathbf{grad} \alpha_{v_1} + \mathbf{grad} \alpha_{v_2}) \\ - \int_{\omega_{\min}}^{\omega_{\max}} \int_D S_n^{A*} \Phi \int_D v (\mathbf{grad}_R \mathbf{W}^A)^t \mathbf{grad}_R \alpha_A \end{bmatrix} + \mathbf{f}(\mathbf{u}_{n-1}, v_{n-1}, \mathbf{A}_{n-1}) \quad (16)$$

$$\text{with } \chi_{uu} = \int_{\omega_{\min}}^{\omega_{\max}} (1 + j\omega\alpha) S_n^{u*} S_n^u d\omega, \delta_{uu} = \int_{\omega_{\min}}^{\omega_{\max}} \omega^2 S_n^{u*} S_n^u d\omega \text{ and}$$

$$\beta_{kl} = \int_{\omega_{\min}}^{\omega_{\max}} S_n^{k*} S_n^l d\omega \text{ for } k, l = \{v, A, u\}.$$

Where α is the damping coefficient and X^* denotes the conjugate of X . In a second step, the functions S_n^l and v_0 are recomputed with the functions \mathbf{R}_n^l supposed to be known. Then, for each $\omega_k \in [\omega_{\min}; \omega_{\max}]$, we have:

$$\begin{bmatrix} (1 + j\omega_k \alpha) \int_D \boldsymbol{\mathcal{D}} \mathbf{R}_n^{u*} \boldsymbol{\mathcal{D}} \mathbf{R}_n^u - \omega_k^2 \int_D \mathbf{R}_n^{u*} \rho \mathbf{R}_n^u & \int_D \boldsymbol{\mathcal{D}} \mathbf{R}_n^{u*} \boldsymbol{\tau}^t \mathbf{grad} \mathbf{R}_n^v & \int_D \boldsymbol{\mathcal{D}} \mathbf{R}_n^{u*} \mathbf{h}^t \mathbf{grad}_R \mathbf{R}_n^A \\ \int_D \mathbf{grad} \mathbf{R}_n^{v*} \boldsymbol{\tau} \boldsymbol{\mathcal{D}} \mathbf{R}_n^u & - \int_D \varepsilon \mathbf{grad} \mathbf{R}_n^{v*} \mathbf{grad} \mathbf{R}_n^v & \mathbf{0} \\ \int_D \mathbf{grad}_R \mathbf{R}_n^{A*} \mathbf{h} \boldsymbol{\mathcal{D}} \mathbf{R}_n^u & \mathbf{0} & \int_D v \mathbf{grad}_R \mathbf{R}_n^{A*} \mathbf{grad}_R \mathbf{R}_n^A \\ \int_D \mathbf{grad} \alpha_{v_1} \boldsymbol{\tau} \boldsymbol{\mathcal{D}} \mathbf{R}_n^u & - \int_D \varepsilon \mathbf{grad} \alpha_{v_1} \mathbf{grad} \mathbf{R}_n^v & \mathbf{0} \end{bmatrix} \begin{bmatrix} S_n^u(\omega_k) \\ S_n^v(\omega_k) \\ S_n^A(\omega_k) \\ v_0(\omega_k) \end{bmatrix} = \begin{bmatrix} \mathbf{0} \\ \mathbf{0} \\ - \Phi \int_D v \mathbf{grad}_R \mathbf{R}_n^{A*} \mathbf{grad}_R \alpha_A \\ Q \end{bmatrix} + \mathbf{g}(\mathbf{u}_{n-1}, v_{n-1}, \mathbf{A}_{n-1}) \quad (17)$$

The two steps are repeated until convergence of all functions \mathbf{R}_n^l , S_n^l and v_0 with $l = \{v, A, u\}$. The number of modes M used to approximate the solutions is not known *a-priori* by the user. Then, a criterion is defined to stop the enrichment process. For example, this criterion can be based on the norm of the n^{th} mode with respect to the norm of the first mode [1] or on quantities of interest [5][7][10]. The convergence of the enrichment process can be improved by introducing an update step of the frequency functions after each calculation of the new mode. This step enables to recompute an optimal subspace of functions orthogonal to the

residual [1]. It consists in recomputing the functions S_j^l for $j \in [1:n]$ with $l = \{v, A, u\}$ and v_0 with respect to the functions R_j^l .

IV. APPLICATION

In term of application, we consider the device presented in Fig. 1 and detailed in [10]. The 2D mesh is composed of 3283 nodes and 6525 triangles. The frequency interval is fixed at $[10^4; 10^5]$ Hz with 401 equidistributed values. The aim is to study the device coupled with an electrical load when the magnetic flux Φ is imposed. The quantities of interest are the voltage between the two electrodes (i.e. equal to $2v_0$) and the maximal deformation along x and y. Then, an Offline/Online approach is used. On the Offline step, a reduced model of the device without load is built applying the PGD presented in section III. On the Online step, the reduced model is coupled with an electrical load in order to study the influence of the load parameters on the quantities of interest.

A. Offline Step: determination of the PGD reduced model

The reduced model is determined by taking advantage of the superposition principle. Two specific configurations of the problem are considered. For each case, approximations of the solutions under the forms given by (10) are computed. For the first configuration, the magnetic flux Φ is imposed and the charge Q is fixed to zero. Then, the PGD formulation presented in the section III is applied. We obtain the PGD approximations: $v_{0\Phi}$, $v_\Phi \approx \sum_{j=1}^M R_{j\Phi}^v(\mathbf{x}) S_{j\Phi}^v(\omega)$, $A_\Phi \approx \sum_{j=1}^M R_{j\Phi}^A(\mathbf{x}) S_{j\Phi}^A(\omega)$

$$\text{and } \mathbf{u}_\Phi \approx \sum_{j=1}^M \mathbf{R}_{j\Phi}^u(\mathbf{x}) S_{j\Phi}^u(\omega).$$

Figure 2 presents the evolutions of the relative error on the electric potential $v_{0\Phi}$ and the maximal deformations $\text{def}_{x\Phi}$ and $\text{def}_{y\Phi}$ along x and y as functions of the number of modes. The relative error is given by

$$\varepsilon_r X = \frac{\|X_{\text{ref}} - X_{\text{pgd}}\|_2}{\|X_{\text{ref}}\|_2} \quad (18)$$

with X the vector of discrete values of quantity of interest (i.e., $v_{0\Phi}$, $\text{def}_{x\Phi}$ or $\text{def}_{y\Phi}$). With a low number of modes, the magnitude of $v_{0\Phi}$ versus the frequency is close to the reference. With $M=5$, the relative error is close to 0.01% and the speed up versus the full model is equal to 8. To obtain good approximations of the maximal deformations, the number of modes must be greater, for $M=16$, we have $\varepsilon_r \text{def}_{x\Phi} < 0.01\%$ and $\varepsilon_r \text{def}_{y\Phi} < 0.01\%$ with a speed up equal to 2.5. Figures 3 and 4 present the evolutions of the voltage magnitude and of the maximal deformation along x and y versus the frequency obtained from the PGD approximations for $M=16$. We can observe a phenomenon of resonance on $v_{0\Phi}$ and $\text{def}_{x\Phi}$ or $\text{def}_{y\Phi}$.

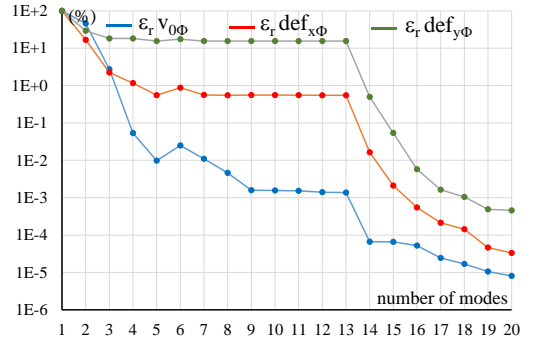


Fig. 2. Relative errors on the electric potential $v_{0\Phi}$ and on the maximal deformations $\text{def}_{x\Phi}$ and $\text{def}_{y\Phi}$ versus the number of modes

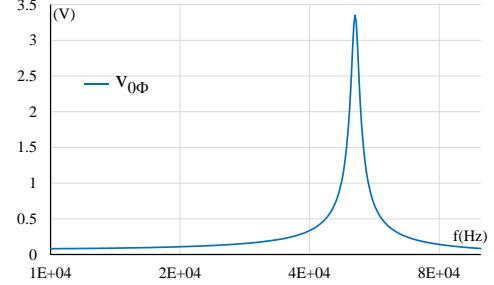


Fig. 3. Magnitude of the voltage versus the frequency.

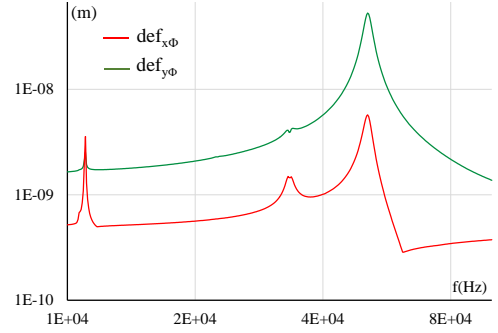


Fig. 4. Maximal deformations along x and y versus the frequency.

For the second configuration, the magnetic flux Φ is fixed to zero, the charge Q is imposed and the PGD approach is applied. The convergence of the PGD is similar to this of the first configuration. As the electric charge Q depends on the electrical load connected to the device, the approximations of the solutions are expressed as functions of Q such as:

$$v_{0Q} Q, v_Q \approx \left(\sum_{j=1}^M R_{jQ}^v(\mathbf{x}) S_{jQ}^v(\omega) \right) Q, A_Q \approx \left(\sum_{j=1}^M R_{jQ}^A(\mathbf{x}) S_{jQ}^A(\omega) \right) Q \text{ and}$$

$$\mathbf{u}_Q \approx \left(\sum_{j=1}^M \mathbf{R}_{jQ}^u(\mathbf{x}) S_{jQ}^u(\omega) \right) Q. \text{ From two specific configurations of}$$

the problem, we can build a reduced model of the device depending on the electric charge. By applying the superposition theorem, the voltage U between the two electrodes, v , \mathbf{A} and \mathbf{u} are expressed by

$$U = 2v_0 = 2v_{0\Phi} + 2v_{0Q}Q \quad (a), \quad v = v_\Phi + v_Q \quad (b), \\ \mathbf{A} = \mathbf{A}_\Phi + \mathbf{A}_Q \quad (c) \text{ and } \mathbf{u} = \mathbf{u}_\Phi + \mathbf{u}_Q \quad (d). \quad (19)$$

B. Online Step: PGD reduced model of the device coupled with electric load

We consider the device coupled with a load composed of a resistor R and of an inductance L (Fig. 5).

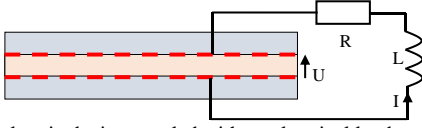


Fig. 5. Magnetolectric device coupled with an electrical load

The device is modeled by the reduced model depending on the electric charge Q . Due to the load, a new coupling equation is added:

$$U + (R + jL\omega)I = 0 \quad \text{with } I = j\omega Q. \quad (20)$$

Then, by combining (19-a) and (20), for each $\omega_k \in [\omega_{\min}; \omega_{\max}]$, $Q(\omega_k)$ is computed by

$$Q(\omega_k) = \frac{-2v_{0\Phi}}{2v_{0Q} + (R + jL\omega_k)j\omega_k} \quad (21)$$

By using (19-b), (19-c) and (19-d) and $Q(\omega_k)$, we can calculate v , \mathbf{A} and \mathbf{u} . \mathbf{E} , \mathbf{B} and \mathbf{S} can be also deduced from (7), (8) and (9). Figure 6 presents the real part of the deformation obtained from the reduced model at the mechanical resonance ($f=73.9\text{kHz}$). Three cases are considered such as the open circuit, $R=4\text{k}\Omega$ and $R=50\Omega$ with $L=10\text{mH}$. Figures 7 and 8 present the evolutions of the voltage magnitude and of the maximal deformation versus the frequency. Then, the maximal magnitude of the voltage decreases when the modulus of the load increases. For the last case ($R=50\Omega$, $L=10\text{mH}$), an electric resonance can be observed on Fig. 7 for a frequency equal to 27.8kHz . This resonance influences the maximal deformations. For all cases, the relative errors on v_0 , def_x or def_y between the full and PGD models are smaller than 0.01% and the speed up is equal to 53. We can see also that, at the contrary to an equivalent electric circuit based on lumped parameters, the link with the full model is kept. In fact, the field distributions can be determined very quickly if necessary from the reduced model. This is not the case with an equivalent circuit which requires, if the field distributions are needed, the solution of the full model.

V. CONCLUSION

The Proper Generalized Decomposition has been applied to a magnetolectric problem to build a reduced model (Offline stage). Then, the PGD reduced model has been coupled with an electric load in order to study the device in its environment during an Online stage. The PGD approach and the use of a reduced model enable to reduce the computational times compared with a full model while maintaining good accuracy and an access to any local and global quantity.

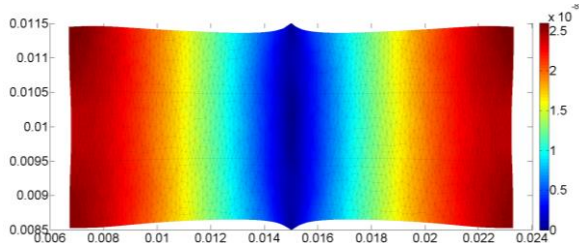


Fig. 6. Real part of the deformation for $f=73.9\text{kHz}$.

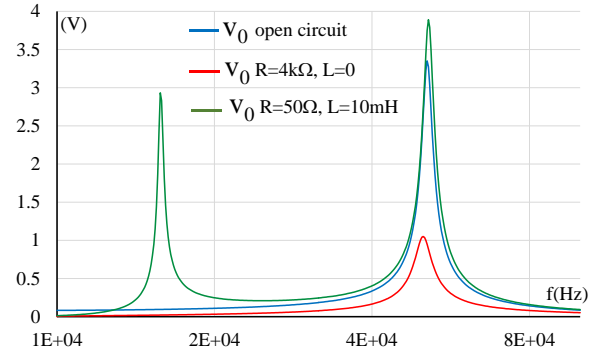


Fig. 7. Magnitude of the voltage versus the frequency for different values of electrical load.

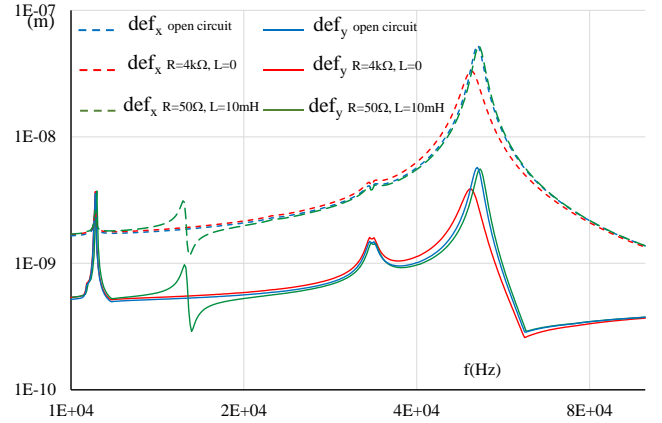


Fig. 8. Maximal deformations along x and y versus the frequency for different values of electrical load.

REFERENCES

- [1] F. Chinesta, R. Keunings and A. Leygue, *The Proper Generalized Decomposition for Advanced Numerical Simulations*, A. Primer, Springer International Publishing, 2014.
- [2] E. Pruliere, F. Chinesta and A. Ammar, "On the deterministic solution of multidimensional parametric models using the Proper Generalized Decomposition", *Numerical Methods in Engineering, Mathematics and Computers in Simulation*, Elsevier, vol. 81 (4), pp.791-810, 2010.
- [3] P. Alotto, M. Guarnieri, F. Moro, A. Stella "A proper generalized decomposition approach for modeling fuel cell polymeric membranes" *IEEE Trans. Mag.*, vol. 47 (5), pp. 1462–1465, 2011.
- [4] T. Henneron, A. Benabou, S. Clénet, "Nonlinear Proper Generalized Decomposition Method Applied to the Magnetic Simulation of a SMC Microstructure", *IEEE Trans. Mag.*, vol. 48(11), pp. 3242-3245, 2012.
- [5] T. Henneron and S. Clénet, "Application of the PGD and DEIM to Solve a 3-D Non-Linear Magnetostatic Problem Coupled With the Circuit Equations", *IEEE Trans. Magn.*, vol. 52, no. 3, 7202104, 2016.
- [6] M. Pineda-Sanchez et al., "Simulation of skin effect via separated representations", *COMPEL*, vol. 29(4), pp.919 – 929, 2010.
- [7] T. Henneron and S. Clénet, "Proper generalized decomposition method applied to solve 3D magnetoquasi-static field problems coupling with external electric circuits", *IEEE Trans. Magn.*, vol. 51, no. 6, pp. 7208910, 2015.
- [8] Z. Qin, H. Talleb and Z.X. Ren, "A proper generalized decomposition based solver for nonlinear magneto-thermal problems", *IEEE Trans. Magn.*, vol. 52, no. 2, pp. 7400209, 2016.
- [9] Z. Qin, H. Talleb, S. Yan and Z.X. Ren, "Application of the PGD in Parametric Finite Element Simulation of a Piezoelectric Energy Harvester", 10th International Symposium on Electric and Magnetic Fields (EMF 2016), (Lyon) France, 2016.
- [10] X. Mingner, H. Talleb and T. Henneron, "Review on Numerical Modeling of Magnetolectric devices", *International Compumag Society Newsletter*, vol. 23(3), 2016.